

Floquet band engineering with Bloch oscillations


Xi Liu,¹ Senmao Tan,² Qing-hai Wang², Longwen Zhou^{3,*} and Jiangbin Gong^{2,4,†}

¹*NUS Graduate School-Integrative Sciences and Engineering Programme (ISEP), National University of Singapore, Singapore 119077, Singapore*

²*Department of Physics, National University of Singapore, Singapore 117551, Singapore*

³*College of Physics and Optoelectronic Engineering, Ocean University of China, Qingdao 266100, China*

⁴*Center for Quantum Technologies, National University of Singapore, Singapore 117543, Singapore*

 (Received 18 August 2022; revised 30 October 2022; accepted 14 December 2022; published 22 December 2022)

This work provides a convenient and powerful means towards the engineering of Floquet bands via Bloch oscillations, by adding a tilted linear potential to periodically driven lattice systems. The added linear field not only restricts the spreading of a time-evolving wave packet but also, depending on the ratio between the Bloch oscillation frequency and the modulation frequency of the periodic driving, dramatically modifies the band profile and topology. Specifically, we consider a driven Aubry-André-Harper model as a working example, in the presence of a linear field. Almost flat Floquet bands or Floquet bands with large Chern numbers due to the interplay between the periodic driving and Bloch oscillations can be obtained, with the band structure and topology extensively tunable by adjusting the ratio of two competing frequencies. To confirm our finding, we further execute the Thouless pumping of one and two interacting bosons in such a lattice system and establish its connection with the topological properties of single- and two-particle Floquet bands.

DOI: [10.1103/PhysRevB.106.224309](https://doi.org/10.1103/PhysRevB.106.224309)

I. INTRODUCTION

Topological Thouless pumping describes the quantized adiabatic transport of particles in a one-dimensional (1D) lattice, which is induced by the slow and time-periodic variation of the lattice potential [1]. It reveals the deep connection among geometric phase, band topology, and quantum adiabatic process [2–6]. The observations of Thouless pumping in setups like cold atoms and photonics not only demonstrate the topology of integer quantum Hall effect from a dynamical perspective, but also provide a powerful tool for the detection of topological invariants through quantum dynamics [7–11].

In the conventional Thouless pump, the applied adiabatic driving field plays the role of a second synthetic dimension [5]. To guarantee the pumping quantization, the initial state of the system needs to be a Wannier state or a uniformly filled Bloch band along the physical dimension, which can be rather challenging to prepare in experiments [8,9]. Recently, Bloch oscillations induced by a linearly tilted potential were found to be able to facilitate the initial state preparation in Thouless pump [12]. Especially, the Bloch oscillations assist in the uniform sampling of eigenstates at all quasimomenta in the first Brillouin zone, so that nearly perfect pumping quantization can be achieved for an arbitrary initial state selected in a band of interest. Adding more interest to studies of Bloch oscillations versus topological phases, Bloch oscillations have also been used in experiments to probe the band topology [13–15]. For systems with many-body inter-

actions, the introduction of a linear potential is also of great interest because a time-evolving state can be localized by such a linear potential due to the so-called Stark many-body localization [16].

Beyond the adiabatic limit, time-periodic driving fields were found to induce rich Floquet topological phases [17–42]. An extension of the Thouless pump to Floquet systems was introduced as a powerful dynamical framework to probe the large Chern number phases of Floquet topological insulators [19,43,44]. However, the Floquet-Thouless pump defined in Ref. [43] requires the system to be prepared in a localized Wannier state or as a uniformly populated Floquet-Bloch band, which is even more challenging to achieve in experiments due to the lack of a Fermi surface in periodically driven systems [45–47]. One may then consider adding a linear potential to a Floquet system, and await the resulting Bloch oscillations to assist the initial state preparation in a Floquet Chern band and thus yielding the quantized Thouless pumping. The actual situation is, however, more subtle and complicated. Indeed, in Floquet systems, once a linear field is introduced, the resulting effective Hamiltonian of the system associated with one whole period of driving is *not* the original effective Hamiltonian plus the linear field under consideration. Qualitatively, this is because of the interplay between the linear field and the microscopic motion within one driving period. Specifically, let $\hat{H}[\theta_1(t)] + \hat{F} = \hat{H}[\theta_1(t + 2\pi/\Omega)] + \hat{F}$ be the time-periodic Hamiltonian of a tight-binding lattice under a linearly tilted potential \hat{F} , where $T_1 = 2\pi/\Omega$ is the Floquet driving period and Ω is the driving frequency. By transforming $\hat{H}[\theta_1(t)] + \hat{F}$ into a rotating frame, the linear potential \hat{F} can be replaced by an oscillating phase factor $\theta_2(t) = \omega_F t$ in the hopping amplitude of the lattice, where

*zhoulw13@u.nus.edu

†phygj@nus.edu.sg

$T_2 = 2\pi/\omega_F$ is the oscillation period and ω_F is the field strength of the linear potential. The rotated Hamiltonian $\widehat{H}_r[\theta_1(t), \theta_2(t)]$ now recovers the translational symmetry along the physical dimension, but as a cost carries two separate time dependencies through the parameters $\theta_1(t)$ and $\theta_2(t)$. If the ratio between the two driving frequencies Ω/ω_F is irrational, the rotated Hamiltonian can no longer describe a Floquet system. When the frequency ratio $\Omega/\omega_F \in \mathbb{Q}$, $\widehat{H}_r[\theta_1(t), \theta_2(t)]$ could still describe a Floquet model, but with a new driving period T that is equal to the least common multiple of T_1 and T_2 . Nevertheless, the two driving fields may couple and interplay strongly in this case, yielding Floquet topological bands and Thouless pumping that are totally different from those that one could expect in the system described by $\widehat{H}[\theta_1(t)]$. Therefore, the impacts of a linearly tilted potential (and its resulting Bloch oscillations) on the topology, initial state preparation, and adiabatic transport in Floquet systems are highly nontrivial and deserve to be explored in detail.

Specifically, the second modulation frequency arising from Bloch oscillations offers three advantages over single-frequency driving to facilitate Floquet engineering. First, the topological band structure of the Floquet system is highly tunable by changing the ratio Ω/ω_F , thus yielding topological phases with large Chern numbers and many chiral edge states. Second, even using a simple initial state such as a Gaussian wave packet which is easier to prepare in experiments, all quasimomentum states within one Floquet band may still be swept rather uniformly. This is an excellent feature because, so far it has been unclear how to achieve such a uniform Floquet band sweeping in Floquet systems due to the lack of a Fermi surface in nonequilibrium systems. Our strategy here may be also useful for the initial state preparation in many-body systems for the study of Floquet-Thouless pumping. Third, the linearly tilted field can localize a time-evolving state and hence greatly suppress its spreading during an adiabatic protocol.

It is also of interest to mention related studies. In Refs. [48–50], the driving frequencies are incommensurate and they are regarded as synthetic dimensions along with the physical dimensions. With this perspective, energy is pumped nonadiabatically from one field to another. In Ref. [51], a driving field on resonance with the Bloch frequency is introduced, mainly to restore the hopping dynamics frozen by the linear field. In Ref. [52], two types of periodic driving with commensurate frequencies were introduced to a cold-atom system to create nontrivial Floquet topological phases. The focus of our work is markedly different. Here we explore how Bloch oscillations can have a large impact on Floquet topological phases and also facilitate Floquet-Thouless pumping. Indeed, we uncover how the Bloch oscillation induced by a linear potential could explicitly modify the topology of quasienergy bands and control the Thouless pumping in a Floquet system. We find that the added linear field could not only restrict the spreading of a time-evolving wave packet, but also dramatically modifies the profile and topology of Floquet bands when the Floquet driving frequency and the linear field strength are set at appropriate rational ratios. Focusing on a driven commensurate Aubry-André-Harper (AAH) model in the presence of a linear field as a working example, we find

almost flat Floquet bands or Floquet bands with large Chern numbers due to the interplay between the periodic driving and Bloch oscillations. The band structures and topology are further found to be highly tunable by adjusting the ratio of two competing frequencies of the fields. To confirm our findings, we further execute the Thouless pumpings of one and two interacting bosons in the system, and establish their connections with the topological properties of single- and two-particle Floquet quasienergy bands.

The rest of the paper is structured as follows. In Sec. II, we introduce a theoretical framework to describe the Floquet band structure and the dynamics of bosons in a 1D superlattice subject to time-periodic driving fields, particle-particle interactions, and an onsite linear potential. In Secs. III and IV, we apply our theory to reveal the Floquet band topology and quantized Thouless pumping in one- and two-particle systems with an emphasis on the role played by the linear potential and the resulting Bloch oscillations. In Sec. V, we summarize our results and discuss potential future directions. Some further calculation details and results are presented in the Appendixes A–C.

II. THEORY

In this section, we introduce the system that we are going to explore and outline the theoretical framework that will be used to study its spectral, topological, and transport features.

A. Hamiltonian and pumping dynamics

We start with a harmonically driven commensurate AAH model [43] plus a linear onsite potential and an interaction term. The resulting Hamiltonian reads as

$$\widehat{H} = \sum_j \left[\frac{J}{2} (\hat{a}_j^\dagger \hat{a}_{j+1} + \text{H.c.}) + V \cos(\lambda j - \beta) \cos(\Omega t) \hat{n}_j \right] + \sum_j \frac{U}{2} \hat{n}_j (\hat{n}_j - 1) + \sum_j \omega_F j \hat{n}_j. \quad (1)$$

Here \hat{a}_j^\dagger (\hat{a}_j) creates (annihilates) a boson on the sublattice site j . J is the hopping amplitude. V is the driving strength. Ω is the driving frequency. ω_F is the strength of linear potential. $\lambda = 2\pi p/q$, with p and q being coprime integers. We choose $p/q = \frac{1}{3}$ in this work, so that the spectrum of \widehat{H} possesses three bands in the absence of the linear potential and many-body interactions. In order to explore topological properties of Floquet bands, we should avoid the integer ratio $p/q \geq 1$ because in this case there will only be one topologically trivial band for the one-particle case. The parameter $\beta \in [0, 2\pi]$ is a phase shift of the superlattice potential, which can be regarded as a quasimomentum along a synthetic dimension [53]. To execute adiabatic pumping, β will be tuned adiabatically from zero to 2π in a pumping protocol.

The reason that we start with a commensurate AAH model is that it forms a paradigm in the study of topological phases and adiabatic transport in both static and Floquet systems [19, 53–62]. Adding a continuous driving term to the AAH model will lead to interesting nonequilibrium topological phases compared to static cases, as shown in a previous study [43]. There, by tuning some system parameters and the driving

frequency, a variety of different Floquet topological phases can be generated. Here, we further introduce a linear potential plus an interaction term to a periodically driven AAH model. The interplay among Bloch oscillations, periodic driving fields, as well as many-particle interactions is expected to take us to new Floquet topological phases, as shown below.

Instead of directly studying the above Hamiltonian in the laboratory frame, we apply a rotation to eliminate the linear potential term, so as to recover translational invariance in real space [63]. The rotation is defined as

$$\widehat{R} = \sum_{|\mathbf{n}\rangle} e^{i\omega_F t \sum_j j n_j} |\mathbf{n}\rangle \langle \mathbf{n}|, \quad (2)$$

following which we get the Hamiltonian in the rotating frame, i.e.,

$$\begin{aligned} \widehat{H}_r = & \sum_j \frac{J}{2} (e^{-i\omega_F t} \hat{a}_j^\dagger \hat{a}_{j+1} + \text{H.c.}) \\ & + \sum_j \left[V \cos(\lambda j - \beta) \cos(\Omega t) \hat{n}_j + \frac{U}{2} \hat{n}_j (\hat{n}_j - 1) \right]. \end{aligned} \quad (3)$$

Note that the above rotating-frame transformation is nothing but a gauge transformation. Because the Bloch oscillations can be induced by an electric field, a magnetic field gradient, or a gravitational force field, etc., it is indeed intuitive to write the system Hamiltonian with a linear potential present, as in Eq. (1). However, the time-dependent hopping in Eq. (3) resulting from a different gauge is useful to the development of theoretical insights. That is, though the two gauges used in Eq. (1) and in Eq. (3) are equivalent, the rotated Hamiltonian in Eq. (3) is more convenient for us to construct initial states such as Wannier states. In our numerical propagation of an initial state in real space, we can directly use the Hamiltonian in Eq. (1).

As shown in Eq. (3), \widehat{H}_r is subject to drivings with two frequencies ω_F and Ω . In order to apply the Floquet formalism, we assume that ω_F and Ω are commensurate, i.e., letting their ratio be a rational number,

$$\omega_F / \Omega = a/b, \quad (4)$$

where a, b are coprime integers. Let $T_1 = 2\pi/\Omega$ and $T_2 = 2\pi/\omega_F$. The smallest common period of the two driving fields is then

$$T = aT_2 = bT_1. \quad (5)$$

Let \mathcal{T} be the time-ordering operator, Floquet operator of the system at each fixed β reads as

$$\widehat{U}(\beta) = \mathcal{T} \exp \left[-i \int_0^T dt \widehat{H}_r(t, \beta) \right]. \quad (6)$$

$\widehat{U}(\beta)$ governs the dynamics of the system over each common driving period of the two-color field. In the next subsection, we discuss how to use the translational invariance of the system to block diagonalize $\widehat{U}(\beta)$ in such a system under the periodic boundary condition (PBC).

B. Multiparticle Floquet-Bloch bands

We now generalize the approaches of Refs. [43,64] to construct multiparticle Floquet-Bloch bands. We consider an

N -particle system with L unit cells. For each cell, we focus on the case with three sublattices. The situations with other numbers of sublattices can be treated in a similar fashion. To simplify the demonstration and without loss of generality, we require N and L to be coprime for $N > 1$. Since $\lambda = 2\pi/3$, the onsite potential term in \widehat{H}_r is a periodic function of period 3. Thus, there are three sublattices in each unit cell. We next define a cotranslation operator \widehat{T}_3 that acts on Fock states as

$$\begin{aligned} \widehat{T}_3 |n_1, n_2, \dots, n_{3L}\rangle \\ = |n_{3L-2}, n_{3L-1}, n_{3L}, n_1, \dots, n_{3(L-1)}\rangle, \end{aligned} \quad (7)$$

i.e., \widehat{T}_3 translates the center of mass of particles over three sublattices to the left under the PBC. One can readily verify that \widehat{T}_3 reduces to the familiar translation operator in the one-particle case. For the rotated Hamiltonian in Eq. (3) and under the PBC, we have

$$\widehat{T}_3 \widehat{H}_r(t, \beta) \widehat{T}_3^\dagger = \widehat{H}_r(t, \beta). \quad (8)$$

For two arbitrary Fock states $|\mathbf{n}_1\rangle$ and $|\mathbf{n}_2\rangle$, there may not exist a $j \in \mathbb{Z}$ such that $|\mathbf{n}_2\rangle = \widehat{T}_3^j |\mathbf{n}_1\rangle$. We define a set S comprising of the so-called seed states [64]. The elements of S include all the Fock states such that any two of them cannot be transformed into each other by \widehat{T}_3^j for any $j \in \mathbb{Z}$. Note that the set S is in fact an equivalence relation. For example, for one-particle case, with a particle on either sublattice of the first unit cell, we get one S comprised of three seed states as $S = \{|1\rangle, |2\rangle, |3\rangle\}$. For a general N , the dimension of Fock space is $D = \binom{3L+N-1}{N}$. Under the assumption that L and N are coprime, each seed state will go back to itself after being acted by \widehat{T}_3 over L times. If L and N are not coprime, the number of actions of \widehat{T}_3 to recover a seed state is not unique, and we will not consider this case. With L and N being coprime, the number of seed states, i.e., the cardinality of set S , is $D_S = D/L$. Because of Eq. (8), \widehat{T}_3 also commutes with $\widehat{U}(\beta)$ and they have common eigenstates $|\psi\rangle$, i.e.,

$$\widehat{U}(\beta) |\psi\rangle = e^{i\epsilon} |\psi\rangle, \quad (9)$$

$$\widehat{T}_3^{-1} |\psi\rangle = e^{i\phi} |\psi\rangle. \quad (10)$$

In the above two equations, ϵ is the quasienergy, whereas ϕ is just the quasimomentum. (In some literature, the quasienergy term is written as $e^{i\epsilon T}$.) Both of them are defined modulo 2π . After some algebra (see Appendix A for more details), we find for any $|\mathbf{m}\rangle \in S$ that

$$e^{i\epsilon} \langle \mathbf{m} | \psi \rangle = \sum_{|\mathbf{n}\rangle \in S} \langle \mathbf{m} | \widehat{U}(\beta) \sum_{j=0}^{L-1} e^{ij\phi} \widehat{T}_3^j |\mathbf{n}\rangle \langle \mathbf{n} | \psi \rangle. \quad (11)$$

Therefore, in order to calculate the quasienergies and eigenstates, we can reduce the full matrix $\widehat{U}(\beta)$ of dimension $D \times D$ to a reduced Floquet operator $\widetilde{U}(\beta, \phi)$ of dimension $D_S \times D_S$, whose matrix elements are

$$\widetilde{U}_{\mathbf{m}\mathbf{n}}(\beta, \phi) = \langle \mathbf{m} | \widehat{U}(\beta) \sum_{j=0}^{L-1} e^{ij\phi} \widehat{T}_3^j |\mathbf{n}\rangle, \quad |\mathbf{m}\rangle, |\mathbf{n}\rangle \in S. \quad (12)$$

The eigenstates of $D_S \times D_S$ matrix $\widetilde{U}(\beta, \phi)$ are given by

$$|\widetilde{\psi}(\beta, \phi)\rangle = [\langle \mathbf{m} | \psi \rangle]_{|\mathbf{m}\rangle \in S}^\top. \quad (13)$$

Here \top means matrix transpose, so that $|\tilde{\psi}(\beta, \phi)\rangle$ is a D_S -dimensional column vector. Note that $|\phi, \mathbf{n}\rangle = \frac{1}{\sqrt{L}} \sum_{j=0}^{L-1} e^{ij\phi} \hat{T}_3^j |\mathbf{n}\rangle$ is just a Bloch eigenstate, and $|\tilde{\psi}(\beta, \phi)\rangle = [(\mathbf{m}|\psi)\rangle]_{|\mathbf{m}\rangle \in S}^\top$ is just the full D -dimensional eigenvector $|\psi\rangle$ from Eqs. (9) and (10) projected over D_S seed states, thus with dimension D_S . By solving this eigenvalue problem, we get D_S quasienergy bands. Note that there is a distinction between one-particle and multiparticle cases. For the one-particle case, the number of bands is always three, i.e., $D_S = 3$, regardless of the value of L . We can use a splitting operator scheme to calculate the 3×3 reduced Floquet operator $\tilde{U}(\beta, \phi)$ for one-particle case, which is much faster than evaluating $\tilde{U}(\beta, \phi)$ for the two-particle case (see the Appendix A of Ref. [65] for more derivation details).

For the two-particle case, the value of D_S changes with L . As long as $D_S \gg 1$, the exact number of bands D_S does not generate a difference in the overall band structure. In the subsequent calculation, we take $L = 21$. The number of bands is thus $D_S = 96$ for $N = 2$, and $D = 2016$. We can then exponentiate the full $D \times D$ Hamiltonian, and multiply these exponentials according to their time ordering. For the one- or two-particle case, the exponential of Hamiltonian is manageable. If we have more particles, the computation will be more challenging as the dimension of the Hamiltonian increases exponentially and quickly becomes computationally prohibitive for exact diagonalization treatments. Once we obtain a reduced eigenvector $|\tilde{\psi}(\beta, \phi)\rangle$ of dimension D_S over seed states, we can recover the D -dimensional full eigenstate $|\psi\rangle$. We also use $|\tilde{\psi}(\beta, \phi)\rangle$ to calculate the Chern number of an isolated band. For the n th band, it is explicitly given by [66]

$$C_n = \int_0^{2\pi} \int_0^{2\pi} \frac{d\beta d\phi}{2\pi i} ((\partial_\beta \tilde{\psi}(\beta, \phi) | \partial_\phi \tilde{\psi}(\beta, \phi)\rangle - \text{H.c.}). \quad (14)$$

Note that for the many-body case, ϕ should be interpreted as the center-of-mass quasimomentum of the particles.

Our pumping scheme uses Wannier and Gaussian states as initial states. Their (unnormalized) expressions are explicitly given by (i) Wannier state

$$|W(R_0, \beta)\rangle = \sum_{\phi} e^{-i\phi R_0} |\psi(\beta, \phi)\rangle, \quad (15)$$

and (ii) Gaussian state

$$|G(R_0, \beta)\rangle = \sum_{\phi} e^{-i\phi R_0 - \frac{1}{4\sigma^2} \phi^2} |\psi(\beta, \phi)\rangle. \quad (16)$$

In the pumping process, we use $|W(R_0, \beta = 0)\rangle$ or $|G(R_0, \beta = 0)\rangle$ as the initial state, and β will be tuned adiabatically over a cycle in the Floquet-Thouless pumping. More precisely, we consider the evolution over a time duration MT with $M \gg 1$ and T the driving period in the pumping dynamics. Within the m th driving period ($m = 1, 2, \dots, M - 1, M$), we let $\beta = 2\pi(m - 1)/M$ and evolve the state using the Hamiltonian in Eq. (1) from $t = (m - 1)T$ to $t = mT$. The pumping is revealed by the expectation value of position operator $\hat{x} = \frac{1}{qN} \sum_j j \hat{n}_j$ at the end of each driving period, with N the particle number. In the construction of Wannier and Gaussian states, we always choose $R_0 = L/2$ for each isolated band, such that the Wannier and Gaussian states are

approximately localized around $L/2$, away from which the amplitude of wave packet is rapidly decreasing in real space. The value $L/2$ is chosen such that during the evolution, the wave packet is always far away from the boundary, and the drift of wave packet center will be quantized. Another choice of R_0 that is close enough to the center of the lattice will also do the job. The Gaussian state in Eq. (16) is constructed in momentum space. Since the Fourier transform of a Gaussian state is again a Gaussian state, Eq. (16) is also a Gaussian state in real space. We choose the width parameter σ such that the wave packet is narrow in both momentum and real spaces. Under this condition, the pumping result is not sensitive to the exact value of σ . In the study of adiabatic pumping, we impose PBC for the rotated Hamiltonian \hat{H}_r . We also obtain the Floquet bands with respect to the phase shift β and center-of-mass quasimomentum $\phi \in [0, 2\pi]$ by diagonalizing the Floquet operator under the PBC. It is also useful to describe how to choose the system parameters in order to find an isolated Floquet band to do Floquet-Thouless adiabatic pumping. In our calculation, we choose $J = V = 2.5$ for all cases. For the one-particle case, we first choose a value of T_1 , and then scan the values of a and b under the constraint that they are coprime integers. Next, we choose the a and b such that all the three Floquet bands are isolated from each other. For the two-particle case, once we fix the value of T_1 , we scan the values of U as well as a and b , with a and b still being coprime integers. We then select the cases where some of the bands are isolated [see Fig. 3(a) for an example, where the topmost band is isolated]. Following our routine, there are many situations in which well-isolated Floquet bands could be found in both one- and two-particle systems. Some representative cases are presented and discussed in detail below.

III. CONTINUOUSLY DRIVEN AAH MODEL WITH ONE BOSON

We first demonstrate the Floquet band engineering in the single-particle case. In this case, we find topological transitions induced by changing the commensurate ratio $\omega_F/\Omega = a/b$ between the two driving frequencies. Moreover, the change of linear potential strength ω_F leads to new topological phases with large Chern numbers and many chiral edge states. We further employ the quantized adiabatic pumping of both Wannier and Gaussian states to reveal the rich Floquet topological properties induced by Bloch oscillations in the system from a dynamical perspective. Throughout this work, we work in dimensionless units and set the system parameters $J = V = 2.5$.

We first present the Floquet bands under the PBC and the adiabatic pumping of Wannier and Gaussian states $|W(R_0, 0)\rangle$ and $|G(R_0, 0)\rangle$ in Figs. 1 and 2, where we take $T_1 = 2$, $a = 3$, and $b = 1$ in Fig. 1, and $T_1 = 4$ in Fig. 2. We observe that the quasienergy bands are flat along the direction of quasimomentum ϕ , as shown in Figs. 1(a) and 2(g). This holds true in other cases with $T_1/T_2 > 1$. The flat dispersion is originated from Bloch oscillations induced by the linear potential. It could lead to the uniform sampling of initial states in momentum space, which is essential for the realization of quantized pumping for an arbitrary single-band state. Regardless of the initial momentum distribution, each state is linearly swept in the

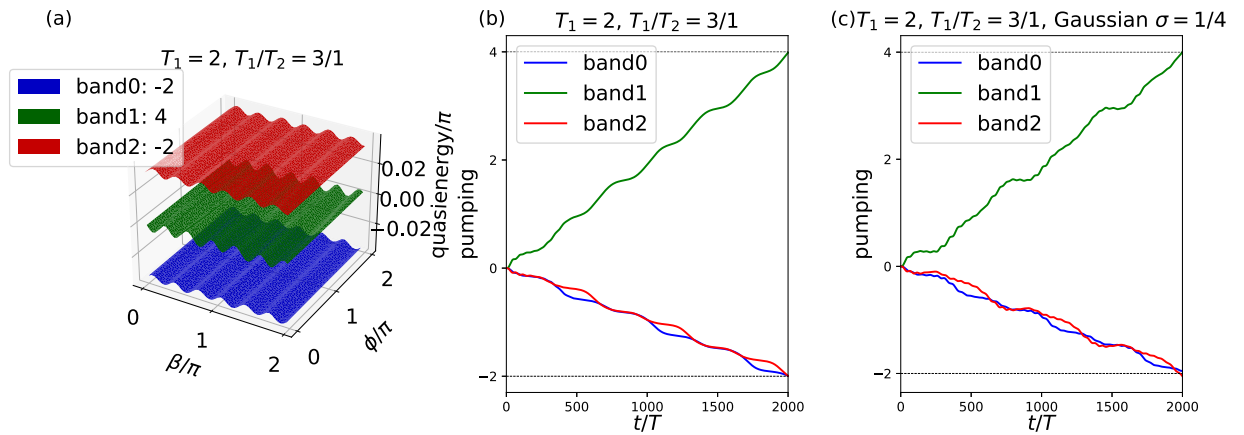


FIG. 1. Floquet spectrum under the PBC, the pumping of Wannier and Gaussian initial states in real space for $T_1 = 2$, $a = 3$, and $b = 1$. (a) The three quasienergy bands with Chern numbers $-2, 4, -2$. (b) Pumping of Wannier states prepared in the three Floquet bands over an adiabatic cycle ($t = 2000T$). (c) Pumping of Gaussian states initialized in the three Floquet bands over an adiabatic cycle ($t = 2000T$). For each Wannier or Gaussian initial state, the shift of wave-packet center over an adiabatic cycle yields the Chern number of the corresponding Floquet band.

momentum space multiple times in a single Floquet period when $T_1/T_2 > 1$, as shown in Appendix B (see Fig. 5), leading to the flat band in the ϕ direction. The easiness of the flat-band generation is one of the benefits of employing the tilted potential, as it allows us to perform the Thouless pumping with arbitrary single-band initial states. To demonstrate the availability of quantized pumping with an arbitrary single-band initial state, we use the Gaussian state as an example. In Figs. 1(b) and 1(c), we show the pumping of Wannier and Gaussian states prepared in the three Floquet bands over an adiabatic cycle consisting of 2000 driving periods. For each case, we observe that the pumping is quantized and the net drift of wave-packet center coincides with the Chern number of the corresponding Floquet band. Importantly, the quantized pumping of Gaussian initial state is made possible due to the flat quasienergy band along the ϕ direction. Compared with the Wannier state, a Gaussian wave packet is easier to prepare in experiments. Therefore, the linear potential provides us with a flexible route to achieve Thouless pumping and measure Chern numbers of Floquet bands in quantum simulators like ultracold atoms in optical lattices.

By changing the strength of the linear potential, the band topology of the system is modified. We consider a group of spectrum and pumping results with other frequency ratios including $\omega_F = 0$, $T_1/T_2 = \frac{2}{5}$ and $\frac{5}{2}$. The Floquet spectrum under the PBC without linear potential is shown in Fig. 2(a) [43]. Here, we observe three dispersive bands with Chern numbers $4, -8, 4$. In Fig. 2(b), the pumping of Wannier states indeed gives the Chern numbers of different Floquet bands. In Figs. 2(d) and 2(e), we turn on the linear potential ω_F such that $T_1/T_2 = \frac{2}{5}$. Interestingly, we see that the curvature of Floquet bands changes dramatically in response to the linear potential, and their Chern numbers could reach values as large as $-20, 40, -20$. Therefore, we could get topological phases with huge Chern numbers by simply changing the value of linear potential strength ω_F . Physically, the Floquet bands with large Chern numbers are originated from the interplay between the Bloch oscillations induced by linear potential and the external periodic driving field. In Fig. 2(g), we take T_1/T_2 as the inverse

of $\frac{2}{5}$. Although the Floquet bands in this case have the same Chern numbers as those in Fig. 2(a), their local band curvatures are totally different. Figure 2(g) has flat band along the ϕ direction, while along ϕ the band in Fig. 2(a) is curved. The pumping results of Wannier states in Fig. 2(h) are consistent with the Chern numbers of the corresponding Floquet bands. We present three more groups of Floquet bands and pumping results by adjusting the ratio of ω_F/Ω in Fig. 6. They indeed show that we can generate rich Floquet topological phases with different frequency ratios ω_F/Ω . For completeness, we show the Floquet spectrum of the system under the OBC in Figs. 2(c), 2(f), and 2(i), and observe that the band Chern numbers correctly predict the number of chiral edge modes traversing the bulk gap at each edge.

Putting together, we conclude that the competition between the periodic driving $e^{\pm i\omega_F t}$ in the hopping terms (due to the linear potential) and the harmonic driving term $\cos(\Omega t)$ (in the onsite superlattice potential) determines the spectral topology and also has a clear impact on the wave-packet dynamics. The interplay between the two driving fields further induces rich topological structures in Floquet bands, leading to quantized adiabatic transport of wave packets over a long spatial range in the lattice due to the large band Chern numbers. The unique feature of this system is that with the driving frequency Ω fixed, by applying a linear field $\sum_j \omega_F j \hat{n}_j$ that breaks the translational invariance of the lattice, the motion of the wave packet can be strongly affected/tuned by Bloch oscillations and exhibits highly nontrivial transport signatures.

Some necessary discussions are in order. First, although the drift in the rotated frame of reference is the same as in the laboratory frame, there is also one subtlety. That is, working with a rotated Hamiltonian via the aforementioned gauge transformation with translational invariance is valid only for states far from the boundary. For this reason, in actual simulations done in real space, we take a sufficiently long lattice and make sure that the wave packet never reaches the boundary of the system. The translational invariance of the rotated Hamiltonian thus becomes valid, yielding the Bloch momentum ϕ to block diagonalize the Floquet operator and to compute

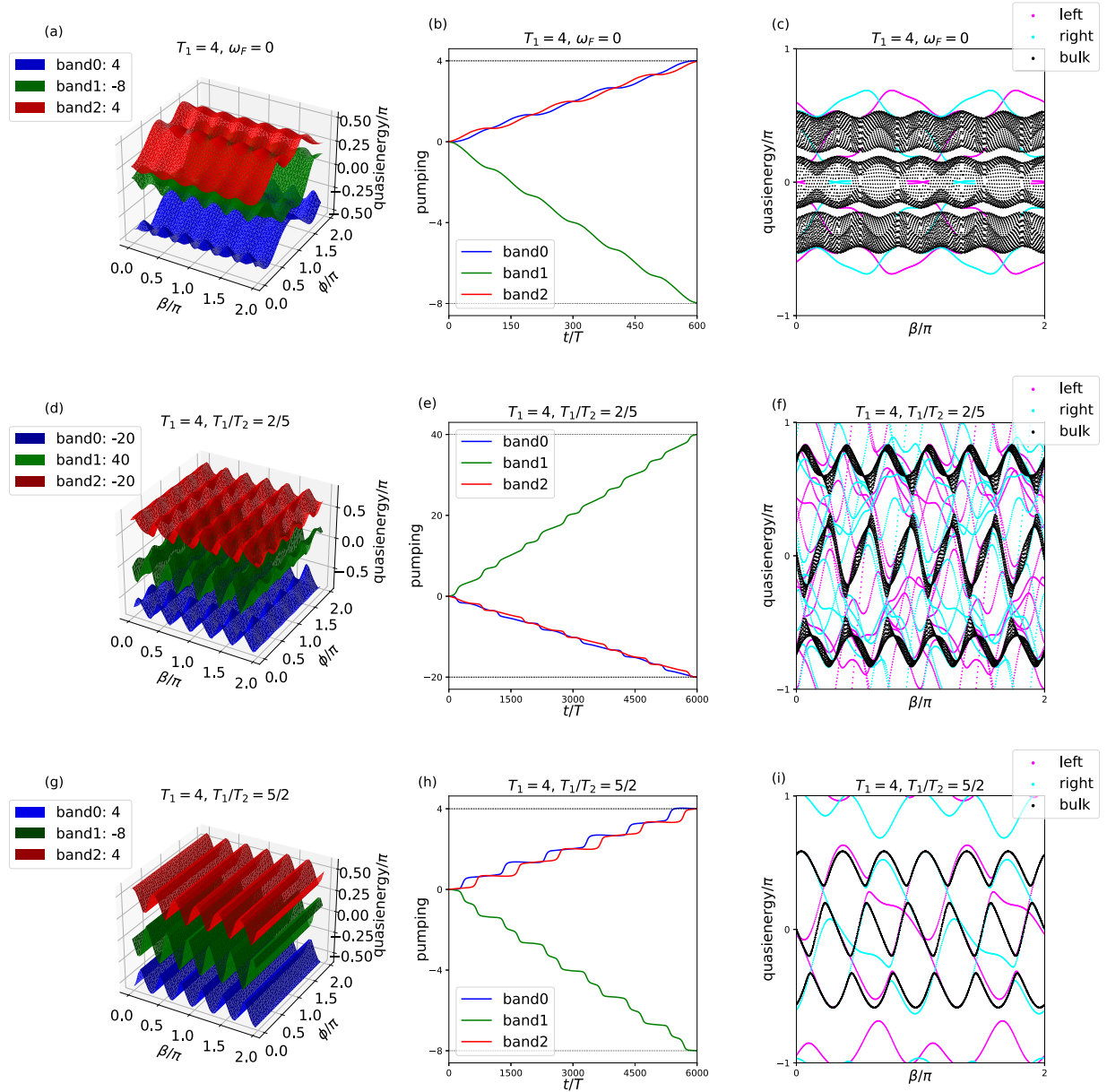


FIG. 2. Floquet spectrum under the PBC, pumping of Wannier states, and Floquet spectrum under the OBC for ($T_1 = 4, \omega_F = 0$) in (a)–(c) and $T_1/T_2 = (\frac{2}{5}, \frac{5}{2})$ in (d)–(i). The legends in (a), (d), and (g) include the Chern numbers of three Floquet bands.

the spectrum. Second, although our work and Ref. [12] have both demonstrated quantized adiabatic pumping under a linear potential, there are notable differences. In Ref. [12], the linear potential assists the uniform sampling in the Brillouin zone, and the quantization of pumping is independent of the strength of linear potential. By contrast, here the strength of the linear field is crucial as it controls the Floquet band topology, leading to rather different pumping results depending on the frequency of the Bloch oscillations induced by the linear field.

IV. CONTINUOUSLY DRIVEN AAH MODEL WITH TWO BOSONS

In this section, we study the Floquet spectrum and Thouless pumping of two interacting bosons in our system. We use the python package QUSPIN [67] to treat the two-boson

case, where exact diagonalization is applied. With two bosons, we have a total of $D_S = 96$ bands under the PBC (still for a unit cell there are three sublattice sites), and it is tedious to visualize all Floquet bands using three-dimensional plots. Therefore, we focus on the Floquet bands obtained along a cut at $\phi = 0$. The band structures obtained at other values of ϕ do not show noteworthy differences. We shall see that rich topological structures of Floquet bands, topological phase transitions, and pumping dynamics can be generated by changing the ratio T_1/T_2 between two driving periods and the interaction strength U . The interplay among the periodic driving, interactions, and Bloch oscillations thus induce nontrivial many-body Floquet topological phases.

The main results of this section are presented in Figs. 3 and 4. In Fig. 3(a), we show the two-particle Floquet spectrum under the PBC for $T_1 = 2, U = 20$, and $T_1/T_2 = \frac{3}{2}$.

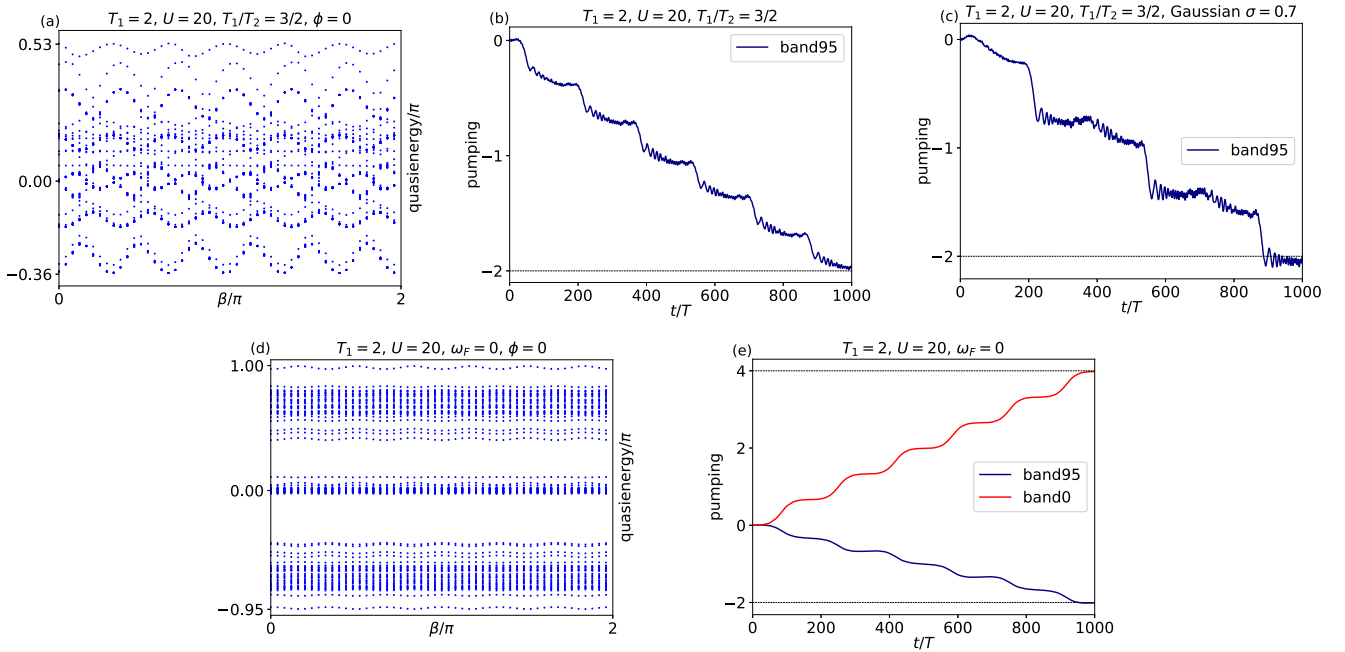


FIG. 3. Floquet spectrum under the PBC and adiabatic pumping of two interacting bosons. The driving period $T_1 = 2$ and interaction strength $U = 20$ are chosen for all panels. (a) Two-particle quasienergy spectrum for $T_1/T_2 = \frac{3}{2}$ along $\phi = 0$. (b) Pumping of a Wannier initial state for $T_1/T_2 = \frac{3}{2}$. (c) Pumping of a Gaussian initial state for $T_1/T_2 = \frac{3}{2}$. (d) Quasienergy spectrum for $\omega_F = 0$ along $\phi = 0$. (e) Pumping of two Wannier initial states for $\omega_F = 0$.

The highest Floquet band (denoted by band 95) is found to be isolated from the rest of spectra. We hence choose to prepare the Wannier and Gaussian initial states on this band. Here Gaussian states refer to a Gaussian profile of the translational state of the center of mass of the bipartite system. Results of our adiabatic pumping using Wannier and Gaussian states as the initial states are shown in Figs. 3(b) and 3(c). The width of the Gaussian state in momentum space is set as $\sigma = 0.7$. We find that the drift of wave-packet center over an adiabatic cycle is the same for the Gaussian and Wannier initial states. They both reproduce the Chern number $C = -2$ of band 95. Therefore, we have successfully observed quantized pumping for two types of initial wave packets. Of particular interest, the quantization of the pumping using only a two-particle Gaussian state is made possible by the linear potential induced Bloch oscillations as in the single-particle case. This indicates that the stage of initial state preparation in Thouless pumping can be greatly simplified even in many-body interacting cases thanks to the Bloch oscillations. As a comparison, we show in Figs. 3(d) and 3(e) the two-particle Floquet bands under the PBC without a linear potential, the pumping of Wannier states prepared on the lowest band (named band 0), and the highest band (named band 95) without the linear potential. The results show that the presence of a linear potential leads to quantized pumping at different integer values. As such, in the case of two interacting bosons, topological phase transitions can be also induced by turning on a linear potential ω_F .

Next, we present four groups of results in Fig. 4 for two-body Floquet spectrum under different boundary conditions, in connection with the quantized two-particle pumping. We set $T_1 = 1$ in all panels of Fig. 4, while choosing the

interaction strengths to be $U = 2, 10$ and setting the ratios of T_1/T_2 as $\frac{1}{1}$ and $\frac{1}{2}$. One goal here is to examine the impact of interaction on the topological pumping. First, comparing the results presented in Figs. 4(a) and 4(g), we see that the decreasing of the ratio T_1/T_2 from $\frac{1}{1}$ to $\frac{1}{2}$ for $U = 2$ makes the lowest band more dispersive. Meanwhile, the number of groups of Floquet bands is kept to be the same as seven. On the other hand, by comparing Figs. 4(d) and 4(j), we see that for $U = 10$ the decreasing of ratio T_1/T_2 from $\frac{1}{1}$ to $1/2$ leads to more apparent differences. Both cases have the highest band (band 95) as an isolated band, while three more isolated bands appear at the bottom in Fig. 4(j), as denoted by bands 0, 1, and 2. The change of interaction strength U also generates significant differences in the spectrum, topological, and transport nature of the system. With the same ratio $T_1/T_2 = \frac{1}{1}$, Figs. 4(a) and 4(d) show the same number of seven groups of bands, but the isolated band goes from the bottom to the top. We can also observe that Fig. 4(a) is similar to the image being turned upside down of Fig. 4(d). Likewise, by comparing the results shown in Figs. 4(g) and 4(j), we see that with the same ratio $T_1/T_2 = \frac{1}{2}$, the number of isolated bands increases from one to four by increasing U from 2 to 10, and the number of groups of bands increases from seven to nine. We conclude that not only the change of the ratio T_1/T_2 , but also the change of the interaction strength U will lead to topological phase transitions in the two-particle system. The Chern numbers in each case of Figs. 4(a), 4(d), 4(g), and 4(j) are obtained by calculating Berry curvatures of Floquet bands under the PBC, and are validated by the quantized two-particle pumpings in Figs. 4(b), 4(e), 4(h), and 4(k). Therefore, we provide concrete examples of topological phase transitions and quantized

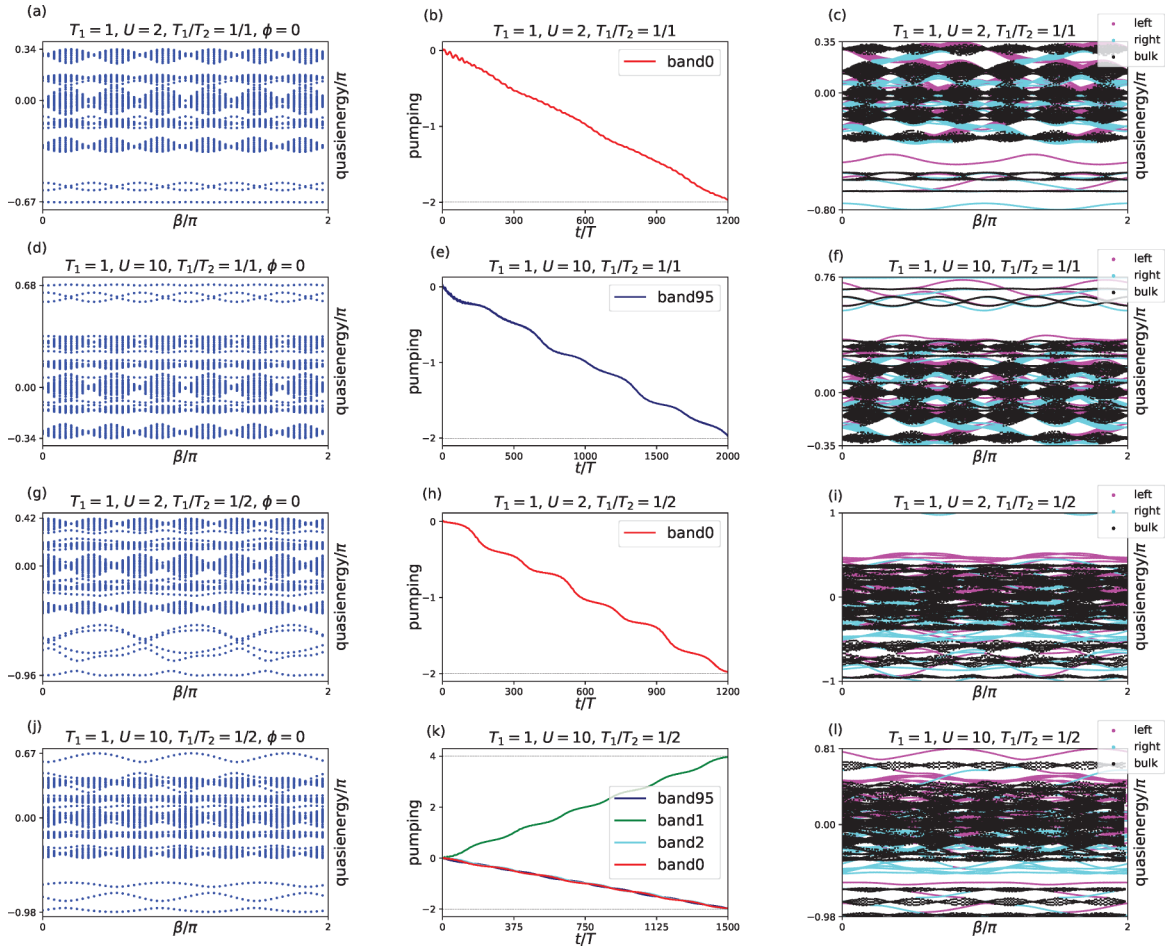


FIG. 4. Floquet spectrum under the PBC along $\phi = 0$ in (a), (d), (g), (j), pumping of Wannier states in (b), (e), (h), (k), and Floquet spectrum under the OBC in (c), (f), (i), (l) for the interaction strengths $U = 2, 10$ and the driving period ratios $T_1/T_2 = \frac{1}{1}, \frac{1}{2}$.

transport in two-particle Floquet systems that are induced by the interplay among a periodic driving field, interactions, and Bloch oscillations.

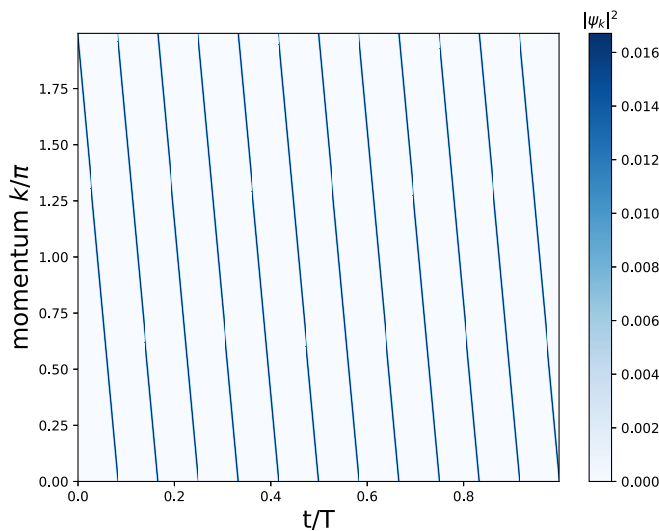


FIG. 5. Time evolution of the single-particle density distribution in momentum space. The chosen parameters are $T = T_1 = 2$, $T_2 = 0.5$, and $J = V = 2.5$.

In Appendix C, we have presented more computational examples. There it is seen that Floquet bands with very high Chern numbers can be obtained by simply adjusting the ratio of the Bloch oscillation frequency to that of the periodic driving. These additional results further strongly indicate that the introduction of a linear field to periodically driven lattices is a powerful means towards Floquet band engineering.

V. DISCUSSION AND SUMMARY

Experimentally, our model and the pumping dynamics may be realized in cold-atom systems. A 1D static AAH model can be realized by superimposing two optical lattices with different lattice constants, which result from standing waves created by retroreflected single-frequency laser beams [68]. To realize the continuously driven AAH model, we may periodically modulate the strength of lattice lasers. The tunable linear field can be generated by a magnetic field gradient along the lattice direction [69]. Different magnetic field gradients lead to different band topologies of the system, thus generating different quantized pumping results.

We have shown that a linear potential applied to a Floquet system can induce quasienergy bands with large Chern

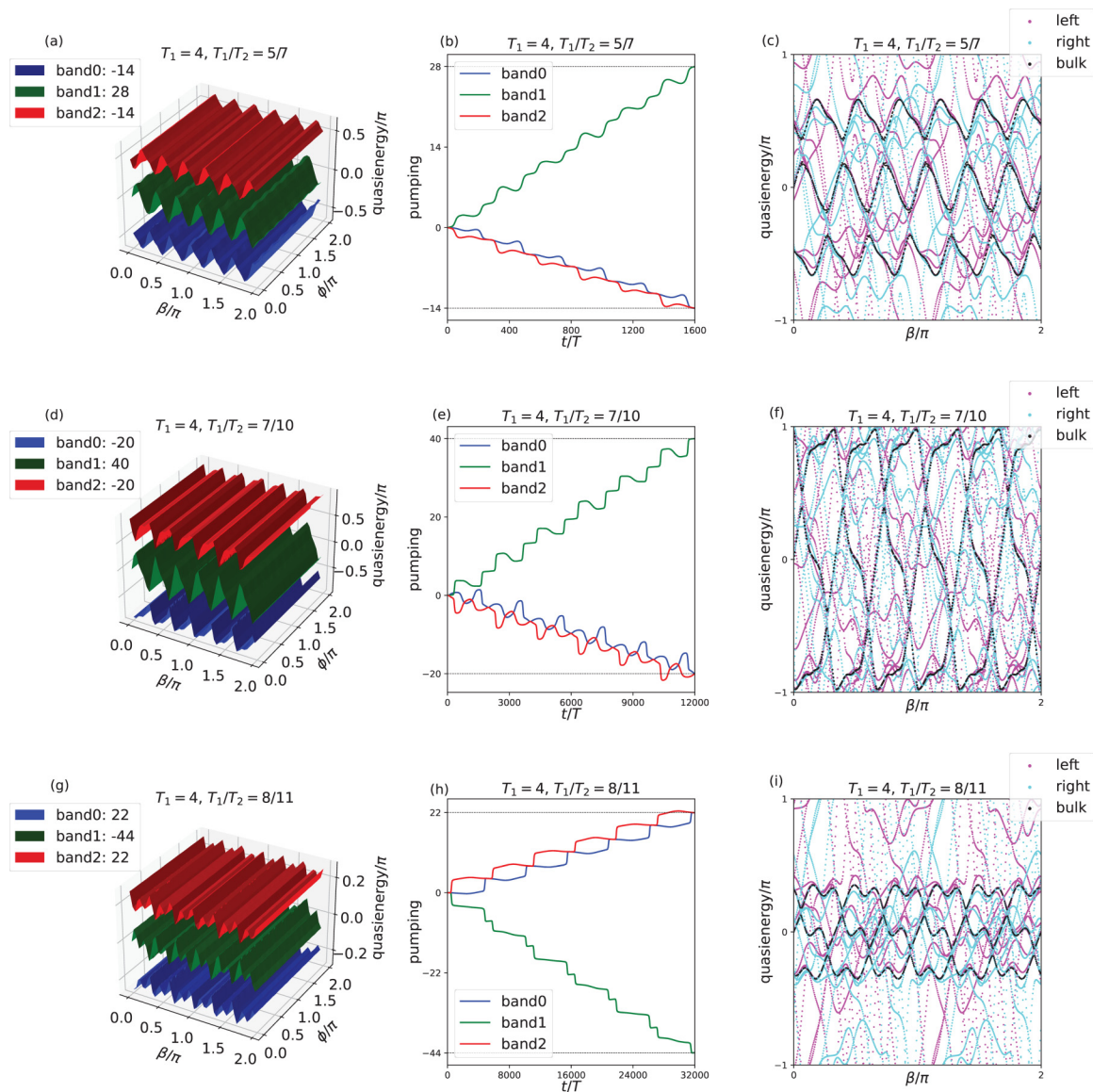


FIG. 6. Floquet bands under the PBC, pumping of Wannier states, and Floquet bands under the OBC for the single-particle case with $T_1 = 4$ and $T_1/T_2 = \frac{5}{7}$ [in (a), (b), (c)], $\frac{7}{10}$ [in (d), (e), (f)], $\frac{8}{11}$ [in (g), (h), (i)], respectively. The legends in (a), (d), and (g) include the Chern numbers of the three Floquet bands.

numbers and rich topological phase transitions. This is verified by calculating the topological invariants as well as adiabatic Thouless pumping of Wannier states. Moreover, we have shown that we can use Gaussian initial states on relatively flat bands to achieve quantized pumping, which is easier to implement in experiments. It is the Bloch oscillation that facilitates the uniform sweeping of eigenstates for such flat bands. Certainly, in Floquet systems, there is no longer uniform sampling of momentum by the Bloch oscillations, as evidenced by the existence of nonflat bands. In these cases, the linear potential can even induce new topological phases. This is the main message from this work, and we hence expect that the introduction of a linear field can be generally useful to the multicolor engineering of Floquet bands [70]. For a two-particle interacting system, not only the ratio of the two driving periods, but also the interaction strength determines the topological phases and hence changes the result of

Floquet-Thouless pumping. In future work, we may consider situations with more bosons or interacting fermions [71], in connection with many-body Stark localization and quantum prethermalization.

ACKNOWLEDGMENTS

L.Z. is supported by the National Natural Science Foundation of China (Grants No. 12275260 and No. 11905211), the Young Talents Project at Ocean University of China (Grant No. 861801013196), and the Applied Research Project of Postdoctoral Fellows in Qingdao (Grant No. 861905040009). J.G. acknowledges support from Singapore National Research Foundation Grant No. NRF-NRFI2017-04 (WBS Grant No. A-0004162-00-00). The computational work for this paper was fully performed on resources of the National Supercomputing Centre, Singapore [72].

APPENDIX A: DERIVATION OF THE FLOQUET EIGENVALUE EQUATION

In this Appendix, we give derivation details of Eq. (11) in the main text. For common eigenstates of the Floquet operator $\widehat{U}(\beta)$ and cotranslation operator \widehat{T}_3^{-1} , we have

$$\widehat{U}(\beta) |\psi\rangle = e^{i\epsilon} |\psi\rangle, \quad (\text{A1})$$

$$\widehat{T}_3^{-1} |\psi\rangle = e^{i\phi} |\psi\rangle. \quad (\text{A2})$$

For the set S of all seed states, the identity operator is

$$\mathbb{1} = \sum_{|\mathbf{n}\rangle \in S} \sum_{j=0}^{L-1} \widehat{T}_3^j |\mathbf{n}\rangle \langle \mathbf{n}| \widehat{T}_3^{-j}. \quad (\text{A3})$$

Then we obtain

$$\begin{aligned} e^{i\epsilon} |\psi\rangle &= \widehat{U}(\beta) |\psi\rangle \\ &= \widehat{U}(\beta) \sum_{|\mathbf{n}\rangle \in S} \sum_{j=0}^{L-1} \widehat{T}_3^j |\mathbf{n}\rangle \langle \mathbf{n}| \widehat{T}_3^{-j} |\psi\rangle \\ &= \sum_{|\mathbf{n}\rangle \in S} \widehat{U}(\beta) \sum_{j=0}^{L-1} e^{ij\phi} \widehat{T}_3^j |\mathbf{n}\rangle \langle \mathbf{n}| \psi\rangle. \end{aligned} \quad (\text{A4})$$

Multiplying $|\mathbf{m}\rangle \in S$ from the left, we get

$$e^{i\epsilon} \langle \mathbf{m}| \psi\rangle = \sum_{|\mathbf{n}\rangle \in S} \langle \mathbf{m}| \widehat{U}(\beta) \sum_{j=0}^{L-1} e^{ij\phi} \widehat{T}_3^j |\mathbf{n}\rangle \langle \mathbf{n}| \psi\rangle. \quad (\text{A5})$$

This is the Eq. (11) in the main text. Note that our scheme of evaluating the reduced Floquet operator in Eq. (12) is equivalent to the Eq. (3) in Ref. [64]. Meanwhile, our scheme has one computational advantage. That is, in order to get each matrix element of \widehat{U} , we do not need to compute matrix-vector products. Instead, we only need to compute the inner product between vectors. Since $\langle \mathbf{m}| \widehat{U}(\beta)$ is a row of $\widehat{U}(\beta)$, we only

need to select this row to perform the inner product with $\sqrt{L} |\phi, \mathbf{n}\rangle = \sum_{j=0}^{L-1} e^{ij\phi} \widehat{T}_3^j |\mathbf{n}\rangle$.

APPENDIX B: EVOLUTION OF PARTICLE DENSITY IN MOMENTUM SPACE

In this Appendix, we provide details for the time evolution of the single-particle density distribution in the momentum space. It allows us to directly observe the effect of Bloch oscillations in Floquet systems. The density distribution is given by

$$|\psi_k|^2 = |\phi_{0,k}|^2 + |\phi_{1,k}|^2 + |\phi_{2,k}|^2, \quad (\text{B1})$$

where for $i = 0, 1, 2$ we have

$$\phi_{i,k} = \frac{1}{\sqrt{L}} \sum_{j=1}^L e^{-ikj} \psi_{j,i}. \quad (\text{B2})$$

In numerical calculations, we choose $L = 500$ as the number of unit cells. In a single Floquet driving period, the momentum is linearly swept through the first Brillouin zone multiple times when $T_1/T_2 > 1$ as shown in Fig. 5, leading to flat quasienergy bands along the direction of the Bloch quasimomentum k .

APPENDIX C: MORE EXAMPLES OF THE SINGLE-PARTICLE SPECTRUM AND PUMPING

In this Appendix, we present three more examples of Floquet quasienergy spectrum and Thouless pumping results in Fig. 6. We can see that by changing the ratio of T_1/T_2 , one can easily obtain topological phases with very high Chern numbers. It is also observed that the actual Chern numbers obtained can be rather sensitive to the strength of the applied linear field. This provides us with more flexibility to control topological phase transitions in Floquet systems.

-
- [1] D. J. Thouless, Quantization of particle transport, *Phys. Rev. B* **27**, 6083 (1983).
- [2] D. J. Thouless, M. Kohmoto, M. P. Nightingale, and M. den Nijs, Quantized Hall Conductance in a Two-Dimensional Periodic Potential, *Phys. Rev. Lett.* **49**, 405 (1982).
- [3] Q. Niu and D. J. Thouless, Quantised adiabatic charge transport in the presence of substrate disorder and many-body interaction, *J. Phys. A: Math. Gen.* **17**, 2453 (1984).
- [4] R. D. King-Smith and D. Vanderbilt, Theory of polarization of crystalline solids, *Phys. Rev. B* **47**, 1651(R) (1993).
- [5] D. Xiao, M.-C. Chang, and Q. Niu, Berry phase effects on electronic properties, *Rev. Mod. Phys.* **82**, 1959 (2010).
- [6] V. Gritsev and A. Polkovnikov, Dynamical quantum hall effect in the parameter space, *Proc. Natl. Acad. Sci. USA* **109**, 6457 (2012).
- [7] L. Wang, M. Troyer, and X. Dai, Topological Charge Pumping in a One-Dimensional Optical Lattice, *Phys. Rev. Lett.* **111**, 026802 (2013).
- [8] M. Lohse, C. Schweizer, O. Zilberberg, M. Aidelsburger, and I. Bloch, A thouless quantum pump with ultracold bosonic atoms in an optical superlattice, *Nat. Phys.* **12**, 350 (2016).
- [9] S. Nakajima, T. Tomita, S. Taie, T. Ichinose, H. Ozawa, L. Wang, M. Troyer, and Y. Takahashi, Topological thouless pumping of ultracold fermions, *Nat. Phys.* **12**, 296 (2016).
- [10] M. Jürgensen, S. Mukherjee, and M. C. Rechtsman, Quantized nonlinear thouless pumping, *Nature (London)* **596**, 63 (2021).
- [11] O. You, S. Liang, B. Xie, W. Gao, W. Ye, J. Zhu, and S. Zhang, Observation of Non-Abelian Thouless Pump, *Phys. Rev. Lett.* **128**, 244302 (2022).
- [12] Y. Ke, S. Hu, B. Zhu, J. Gong, Y. Kivshar, and C. Lee, Topological pumping assisted by bloch oscillations, *Phys. Rev. Res.* **2**, 033143 (2020).
- [13] L. Duca, T. Li, M. Reitter, I. Bloch, M. Schleier-Smith, and U. Schneider, An aharonov-bohm interferometer for determining bloch band topology, *Science* **347**, 288 (2015).
- [14] M. Aidelsburger, M. Lohse, C. Schweizer, M. Atala, J. T. Barreiro, S. Nascimbène, N. R. Cooper, I. Bloch, and N. Goldman, Measuring the chern number of hofstadter bands with ultracold bosonic atoms, *Nat. Phys.* **11**, 162 (2015).

- [15] M. Atala, M. Aidelsburger, J. T. Barreiro, D. Abanin, T. Kitagawa, E. Demler, and I. Bloch, Direct measurement of the zak phase in topological bloch bands, *Nat. Phys.* **9**, 795 (2013).
- [16] M. Schulz, C. A. Hooley, R. Moessner, and F. Pollmann, Stark Many-Body Localization, *Phys. Rev. Lett.* **122**, 040606 (2019).
- [17] T. Oka and H. Aoki, Photovoltaic hall effect in graphene, *Phys. Rev. B* **79**, 081406(R) (2009).
- [18] N. H. Lindner, G. Refael, and V. Galitski, Floquet topological insulator in semiconductor quantum wells, *Nat. Phys.* **7**, 490 (2011).
- [19] D. Y. H. Ho and J. Gong, Quantized Adiabatic Transport In Momentum Space, *Phys. Rev. Lett.* **109**, 010601 (2012).
- [20] J. Cayssol, B. Dóra, F. Simon, and R. Moessner, Floquet topological insulators, *Phys. Status Solidi RRL* **7**, 101 (2013).
- [21] A. G. Grushin, Á. Gómez-León, and T. Neupert, Floquet Fractional Chern Insulators, *Phys. Rev. Lett.* **112**, 156801 (2014).
- [22] P. Titum, N. H. Lindner, M. C. Rechtsman, and G. Refael, Disorder-Induced Floquet Topological Insulators, *Phys. Rev. Lett.* **114**, 056801 (2015).
- [23] D. Leykam, M. C. Rechtsman, and Y. D. Chong, Anomalous Topological Phases and Unpaired Dirac Cones in Photonic Floquet Topological Insulators, *Phys. Rev. Lett.* **117**, 013902 (2016).
- [24] L. Zhou, C. Chen, and J. Gong, Floquet semimetal with floquet-band holonomy, *Phys. Rev. B* **94**, 075443 (2016).
- [25] R. Roy and F. Harper, Periodic table for floquet topological insulators, *Phys. Rev. B* **96**, 155118 (2017).
- [26] R. W. Bomantara and J. Gong, Simulation of Non-Abelian Braiding in Majorana Time Crystals, *Phys. Rev. Lett.* **120**, 230405 (2018).
- [27] M. Rodríguez-Vega and B. Seradjeh, Universal Fluctuations of Floquet Topological Invariants at Low Frequencies, *Phys. Rev. Lett.* **121**, 036402 (2018).
- [28] H. H. Yap, L. Zhou, C. H. Lee, and J. Gong, Photoinduced half-integer quantized conductance plateaus in topological-insulator/superconductor heterostructures, *Phys. Rev. B* **97**, 165142 (2018).
- [29] L. Zhou and J. Gong, Floquet topological phases in a spin-1/2 double kicked rotor, *Phys. Rev. A* **97**, 063603 (2018).
- [30] L. Zhou and J. Gong, Recipe for creating an arbitrary number of floquet chiral edge states, *Phys. Rev. B* **97**, 245430 (2018).
- [31] K. Yang, L. Zhou, W. Ma, X. Kong, P. Wang, X. Qin, X. Rong, Y. Wang, F. Shi, J. Gong, and J. Du, Floquet dynamical quantum phase transitions, *Phys. Rev. B* **100**, 085308 (2019).
- [32] R. W. Bomantara, L. Zhou, J. Pan, and J. Gong, Coupled-wire construction of static and floquet second-order topological insulators, *Phys. Rev. B* **99**, 045441 (2019).
- [33] M. S. Rudner and N. H. Lindner, Band structure engineering and non-equilibrium dynamics in floquet topological insulators, *Nat. Rev. Phys.* **2**, 229 (2020).
- [34] S. Afzal, T. J. Zimmerling, Y. Ren, D. Perron, and V. Van, Realization of Anomalous Floquet Insulators in Strongly Coupled Nanophotonic Lattices, *Phys. Rev. Lett.* **124**, 253601 (2020).
- [35] K. Wintersperger, C. Braun, F. N. Únal, A. Eckardt, M. D. Liberto, N. Goldman, I. Bloch, and M. Aidelsburger, Realization of an anomalous floquet topological system with ultracold atoms, *Nat. Phys.* **16**, 1058 (2020).
- [36] J. W. McIver, B. Schulte, F.-U. Stein, T. Matsuyama, G. Jotzu, G. Meier, and A. Cavalleri, Light-induced anomalous hall effect in graphene, *Nat. Phys.* **16**, 38 (2020).
- [37] S. Tan, R. W. Bomantara, and J. Gong, High-fidelity and long-distance entangled-state transfer with floquet topological edge modes, *Phys. Rev. A* **102**, 022608 (2020).
- [38] L. Zhou and Q. Du, Floquet topological phases with fourfold-degenerate edge modes in a driven spin-1/2 creutz ladder, *Phys. Rev. A* **101**, 033607 (2020).
- [39] R. W. Bomantara and J. Gong, Measurement-only quantum computation with floquet majorana corner modes, *Phys. Rev. B* **101**, 085401 (2020).
- [40] W. Zhu, M. Umer, and J. Gong, Floquet higher-order weyl and nexus semimetals, *Phys. Rev. Res.* **3**, L032026 (2021).
- [41] W. Zhu, Y. D. Chong, and J. Gong, Symmetry analysis of anomalous floquet topological phases, *Phys. Rev. B* **104**, L020302 (2021).
- [42] C. Chen, X. Ding, J. Qin, J. Wu, Y. He, C.-Y. Lu, L. Li, X.-J. Liu, B. C. Sanders, and J.-W. Pan, Topological Spin Texture of Chiral Edge States in Photonic Two-Dimensional Quantum Walks, *Phys. Rev. Lett.* **129**, 046401 (2022).
- [43] L. Zhou, H. Wang, D. Y. H. Ho, and J. Gong, Aspects of floquet bands and topological phase transitions in a continuously driven superlattice, *Eur. Phys. J. B* **87**, 204 (2014).
- [44] T.-S. Xiong, J. Gong, and J.-H. An, Towards large-chern-number topological phases by periodic quenching, *Phys. Rev. B* **93**, 184306 (2016).
- [45] H. Wang, L. Zhou, and J. Gong, Interband coherence induced correction to adiabatic pumping in periodically driven systems, *Phys. Rev. B* **91**, 085420 (2015).
- [46] G. N. Raghava, L. Zhou, and J. Gong, Interband coherence induced correction to thouless pumping: Possible observation in cold-atom systems, *Eur. Phys. J. B* **90**, 143 (2017).
- [47] W. Ma, L. Zhou, Q. Zhang, M. Li, C. Cheng, J. Geng, X. Rong, F. Shi, J. Gong, and J. Du, Experimental Observation of a Generalized Thouless Pump with a Single Spin, *Phys. Rev. Lett.* **120**, 120501 (2018).
- [48] D. M. Long, P. J. D. Crowley, and A. Chandran, Nonadiabatic Topological Energy Pumps with Quasiperiodic Driving, *Phys. Rev. Lett.* **126**, 106805 (2021).
- [49] Z. Qi, G. Refael, and Y. Peng, Universal nonadiabatic energy pumping in a quasiperiodically driven extended system, *Phys. Rev. B* **104**, 224301 (2021).
- [50] F. Nathan, R. Ge, S. Gazit, M. Rudner, and M. Kolodrubetz, Quasiperiodic Floquet-Thouless Energy Pump, *Phys. Rev. Lett.* **127**, 166804 (2021).
- [51] M. Aidelsburger, M. Atala, S. Nascimbène, S. Trotzky, Y.-A. Chen, and I. Bloch, Experimental Realization of Strong Effective Magnetic Fields in an Optical Lattice, *Phys. Rev. Lett.* **107**, 255301 (2011).
- [52] A. Quelle, C. Weitenberg, K. Sengstock, and C. M. Smith, Driving protocol for a floquet topological phase without static counterpart, *New J. Phys.* **19**, 113010 (2017).
- [53] L. Lang, X. Cai, and S. Chen, Edge States and Topological Phases in One-Dimensional Optical Superlattices, *Phys. Rev. Lett.* **108**, 220401 (2012).
- [54] Q. Lin, T. Li, L. Xiao, K. Wang, W. Yi, and P. Xue, Topological Phase Transitions and Mobility Edges in Non-Hermitian Quasicrystals, *Phys. Rev. Lett.* **129**, 113601 (2022).
- [55] S. Hu, Y. Ke, Y. Deng, and C. Lee, Dispersion-suppressed topological thouless pumping, *Phys. Rev. B* **100**, 064302 (2019).

- [56] T.-S. Zeng, W. Zhu, and D. N. Sheng, Fractional charge pumping of interacting bosons in one-dimensional superlattice, *Phys. Rev. B* **94**, 235139 (2016).
- [57] F. Liu, S. Ghosh, and Y. D. Chong, Localization and adiabatic pumping in a generalized Aubry-André-Harper model, *Phys. Rev. B* **91**, 014108 (2015).
- [58] M. Verbin, O. Zilberberg, Y. Lahini, Y. E. Kraus, and Y. Silberberg, Topological pumping over a photonic fibonacci quasicrystal, *Phys. Rev. B* **91**, 064201 (2015).
- [59] M. Verbin, O. Zilberberg, Y. E. Kraus, Y. Lahini, and Y. Silberberg, Observation of Topological Phase Transitions in Photonic Quasicrystals, *Phys. Rev. Lett.* **110**, 076403 (2013).
- [60] S. Ganeshan, K. Sun, and S. Das Sarma, Topological Zero-Energy Modes in Gapless Commensurate Aubry-André-Harper Models, *Phys. Rev. Lett.* **110**, 180403 (2013).
- [61] F. Grusdt, M. Hönig, and M. Fleischhauer, Topological Edge States in the One-Dimensional Superlattice Bose-Hubbard Model, *Phys. Rev. Lett.* **110**, 260405 (2013).
- [62] Y. E. Kraus and O. Zilberberg, Topological Equivalence between the Fibonacci Quasicrystal and the Harper Model, *Phys. Rev. Lett.* **109**, 116404 (2012).
- [63] A. Eckardt, Colloquium: Atomic quantum gases in periodically driven optical lattices, *Rev. Mod. Phys.* **89**, 011004 (2017).
- [64] Y. Ke, X. Qin, Y. S. Kivshar, and C. Lee, Multiparticle Wannier states and Thouless pumping of interacting bosons, *Phys. Rev. A* **95**, 063630 (2017).
- [65] H. Wang, D. Y. H. Ho, W. Lawton, J. Wang, and J. Gong, Kicked-harper model versus on-resonance double-kicked rotor model: From spectral difference to topological equivalence, *Phys. Rev. E* **88**, 052920 (2013).
- [66] J. K. Asbóth, L. Oroszlány, and A. Pályi, *A Short Course on Topological Insulators* (Springer, Cham, 2016).
- [67] P. Weinberg and M. Bukov, QuSpin: A python package for dynamics and exact diagonalisation of quantum many body systems. part II: Bosons, fermions and higher spins, *SciPost Phys.* **7**, 020 (2019).
- [68] M. Schreiber, S. S. Hodgman, P. Bordia, H. P. Lüschen, M. H. Fischer, R. Vosk, E. Altman, U. Schneider, and I. Bloch, Observation of many-body localization of interacting fermions in a quasirandom optical lattice, *Science* **349**, 842 (2015).
- [69] Z. A. Geiger, K. M. Fujiwara, K. Singh, R. Senaratne, S. V. Rajagopal, M. Lipatov, T. Shimasaki, R. Driben, V. V. Konotop, T. Meier *et al.*, Observation and Uses of Position-Space Bloch Oscillations in an Ultracold Gas, *Phys. Rev. Lett.* **120**, 213201 (2018).
- [70] S. Zhang and J. Gong, Floquet engineering with particle swarm optimization: Maximizing topological invariants, *Phys. Rev. B* **100**, 235452 (2019).
- [71] S. Mu, D.-J. Zhang, L. Zhou, and J. Gong, Revealing many-body effects on interband coherence through adiabatic charge pumping, *Phys. Rev. B* **100**, 144303 (2019).
- [72] See <https://www.nscg.sg>.